Crystal Structure of *Saccharomyces cerevisiae* 3′-Phosphoadenosine-5′-phosphosulfate Reductase Complexed with Adenosine 3′,5′-Bisphosphate[†,‡]

Zhihao Yu,[§] Donna Lemongello,[||,⊥] Irwin H. Segel,[||] and Andrew J. Fisher*[,§,||]

Departments of Chemistry and Molecular and Cellular Biology, University of California, Davis, One Shields Avenue, Davis, California 95616

Received June 13, 2008; Revised Manuscript Received September 25, 2008

ABSTRACT: Most assimilatory bacteria, fungi, and plants species reduce sulfate (in the activated form of APS or PAPS) to produce reduced sulfur. In yeast, PAPS reductase reduces PAPS to sulfite and PAP. Despite the difference in substrate specificity and catalytic cofactor, PAPS reductase is homologous to APS reductase in both sequence and structure, and they are suggested to share the same catalytic mechanism. Metazoans do not possess the sulfate reduction pathway, which makes APS/PAPS reductases potential drug targets for human pathogens. Here, we present the 2.05 Å resolution crystal structure of the yeast PAPS reductase binary complex with product PAP bound. The N-terminal region mediates dimeric interactions resulting in a unique homodimer assembly not seen in previous APS/PAPS reductase structures. The "pyrophosphate-binding" sequence ^{47}TTAFGLTG^{54} defines the substrate 3′-phosphate binding pocket. In yeast, Gly54 replaces a conserved aspartate found in APS reductases vacating space and charge to accommodate the 3′-phosphate of PAPS, thus regulating substrate specificity. Also, for the first time, the complete C-terminal catalytic motif ^{244}ECGIH^{248} is revealed in the active site. The catalytic residue Cys245 is ideally positioned for an in-line attack on the β-sulfate of PAPS. In addition, the side chain of His248 is only 4.2 Å from the Sγ of Cys245 and may serve as a catalytic base to deprotonate the active site cysteine. A hydrophobic sequence ^{252}RFAQFL^{257} at the end of the C-terminus may provide anchoring interactions preventing the tail from swinging away from the active site as seen in other APS/PAPS reductases.

Sulfate (SO_4^{2-}) is the main source of reduced sulfur for most assimilatory bacteria, fungi, and plant species. In these organisms, sulfate (oxidation state +6) is reduced to sulfite (oxidation state +4) and then to sulfide (oxidation state −2) in order to synthesize reduced sulfur compounds, e.g., cysteine (*1*). The first sulfate/sulfite reduction potential $E^{\circ\prime}$ is −516 mV, which is too low to be carried out by biological systems (*2*). Activation of the sulfate by coupling it to ATP to generate APS[1] or PAPS increases the reduction potential to a more biologically manageable $E^{\circ\prime} = -60$ mV. Sulfate is first activated to APS from ATP and SO_4^{2-}. This reaction is catalyzed by the enzyme ATP sulfurylase, a reaction that is thermodynamically unfavorable ($K_{eq} = 10^{-7}$) (*3*−*6*). APS can be phosphorylated by APS kinase to generate PAPS, the universal sulfate donor (*7*).

In plants, algae, and many Gram-positive bacteria, APS enters in the sulfur reduction pathway where APS reductase produces sulfite and AMP (*8, 9*). Yet in most Gram-negative enteric bacteria and fungi, PAPS reductase reduces PAPS to sulfite and PAP (*10, 11*). While these two classes of sulfate-reducing enzymes display sequence homology, one distinction between the enzymes is the presence of a [4Fe-4S] center binding to a conserved CC-X$_{\sim 80}$-CXXC motif in APS reductase, which not observed in PAPS reductase (*10*). Despite the difference in substrate specificity and catalytic cofactor, the two classes of sulfate reducing enzymes are homologous in both sequences and structures (*10, 12, 13*) and are suggested to share the same catalytic mechanism (*14*). In the proposed two-step ping-pong mechanism, an active site cysteine, near the C-terminus of the reductase, attacks the sulfate group on the sulfonucleotide to produce an enzyme-thiosulfonate intermediate (Cys-S-SO_3^-) plus nucleotide (AMP or PAP). The C-terminal tail then swings out of the active site and interacts with thioredoxin, where the Cys-thiosulfonate intermediate is reduced to sulfite plus cysteine (*14*−*16*). The [4Fe-4S] cluster in APS reductase

[†] This work supported in part by NSF Grant MCB-0515352 to A.J.F. and I.H.S. and the W. M. Keck Foundation Center for Structural Biology at the University of California, Davis.

[‡] Protein coordinates have been deposited in the Protein Data Bank (http://www.rcsb.org/pdb/), accession code 2OQ2.

* Corresponding author. Tel: (530) 754-6180. Fax: (530) 752-8995. E-mail: fisher@chem.ucdavis.edu.

[§] Department of Chemistry, University of California, Davis.

[||] Department of Molecular and Cellular Biology, University of California, Davis.

[⊥] Present address: Department of Medical Microbiology and Immunology, School of Medicine, University of California, Davis, One Shields Ave., Davis, CA 95616.

[1] Abbreviations: ASU, asymmetric unit, APS, adenosine 5′-phosphosulfate (adenylyl sulfate); PAPS, 3′-phosphoadenosine 5′-phosphosulfate (adenylyl sulfate 3′-phosphate); PAP, adenosine 3′,5′-bisphosphate; Tris, tris(hydroxymethyl)aminomethane; TCEP, tris(2-carboxyethyl)phosphine; DTT, dithiothreitol; MAD, multiple wavelength anomalous dispersion; rmsd, root mean square deviation; SSRL, Stanford Synchrotron Radiation Laboratory.

10.1021/bi801118f CCC: $40.75
Published on Web 11/08/2008

appears to be required for activity (*17, 18*). Resonance Raman spectra suggest the cluster interacts with the APS (*18, 19*), yet the recent crystal structure of APS reductase from *Pseudomonas* reveals a distance of >6.5 Å between the sulfate moiety and the [4Fe-4S] cluster (*12*). The absence of the [4Fe-4S] cluster in PAPS reductase, which presumes a similar catalytic mechanism, suggests the [4Fe-4S] cluster in APS reductase may not be directly involved in electron transfer but may be important for regulating the reduction potential in the active site.

APS reductase from dissimilatory sulfate-reducing and sulfate-oxidizing prokaryotes differs substantially from PAPS/APS reductase in sulfur assimilating organisms. The dissimilatory APS reductase is heterodimeric with a FAD-containing α subunit and two [4Fe-4S] clusters in a β subunit (*20, 21*). Additionally, the mechanism is unlike the assimilating reductase and involves a FAD-sulfite adduct with the electrons transferred through the [4Fe-4S] clusters (*22*).

Metazoans do not possess the sulfate reduction pathway because they acquire reduced sulfur directly from their diet. Thus, it has been proposed that the inhibitors of APS/PAPS reductases could be potential drug candidates since APS/PAPS reductase genes were found to be essential for the viability of human pathogens, e.g., *Mycobacterium tuberculosis* (*23*). Therefore, it is important to accumulate mechanistic and structural information of APS/PAPS reductase to guide the rational therapeutic development.

Previous crystal structures of these enzymes have been recently reported, which have been instrumental in helping to better understand the sulfur reduction mechanism. The crystal structure of *Escherichia coli* PAPS reductase in the absence of any substrate/product revealed the fold, but the C-terminal tail containing the conserved active site ECG(I/L)H motif was disordered (*13*). The crystal structure of *Pseudomonas aeruginosa* APS reductase complexed with substrate APS was determined, revealing that it assembled as a homotetramer with APS bound in two of four active sites (*12*). While this structure confirmed the [4Fe-4S] cluster and APS binding site, it too failed to reveal the active site C-terminal tail. Recently, the crystal structure of *E. coli* PAPS reductase trapped in complex with thioredoxin revealed a catalytic snapshot of the intermolecular disulfide bond between the two proteins (*16*). This structure revealed the C-terminal tail extended outside of the active site pocket, where it covalently bound to thioredoxin, but the structure did not reveal details of PAPS binding in the active site pocket nor the conformation of the C-terminal tail in the active site. We report here the crystal structure of a eukaryotic PAPS reductase from yeast with product PAP bound. The structure reveals, for the first time, the complete intact C-terminal tail bound over the active site pocket and provides additional clues to the catalytic mechanism.

EXPERIMENTAL PROCEDURES

Cloning and Site-Directed Mutagenesis. The gene encoding PAPS reductase (GenBank accession number NC_001148) was amplified from genomic DNA of yeast strain CRY1 by the polymerase chain reaction using the proofreading Vent DNA polymerase (New England Biolabs). The primers used were 5′-CCGAGTGCATATGAAGACCTACCATTTGAATAATG-3′ (upstream) and 5′-GATCCCCGGGGGCATCTTGCTTTAAAAATTGCGC-3′ (downstream). The cloned gene was inserted into the pTYB2 plasmid (New England Biolabs) utilizing the restriction sites *Nde*I and *Sma*I.

Protein Expression and Purification. The PAPS reductase was expressed in *E. coli* BL21-CodonPlus (Stratagene) cells grown in 6 L of LB-rich medium (containing 10 g/L tryptone, 5 g/L yeast extract, and 10 g/L NaCl) with 100 μg/mL ampicillin at 37 °C. The temperature was lowered to 15 °C once the A_{600nm} reached 0.8−1.0 unit. After the 30 min incubation, α-lactose (1 g/L of LB) was added to induce protein expression, which normally last for 12−16 h. The bacterial cells were harvested by centrifugation at 4 °C in a fixed angle centrifuge (Beckman) at 5000*g* for 15 min. The cell pellet was resuspended in binding buffer (50 mM Tris-HCl, 500 mM NaCl, 0.1% Triton X-100, pH 8.0). Cells were lysed by one pass through a microfluidizer (Microfluidics, Inc.) at 15000 psi and clarified by centrifugation for 30 min at 35000*g* at 4 °C. Supernatant was loaded onto a column packed with chitin beads (New England Biolabs) and washed extensively with the binding buffer and then the washing buffer (binding buffer without Triton X-100). The protein was cleaved off the intein/CDB domain by an overnight incubation in washing buffer containing 50 mM DTT. The protein was eluted from the column with washing buffer, and the fractions containing the target protein were pooled and dialyzed against 0.1 mM DTT and 50 mM Tris-HCl buffer, pH 8.0.

Preparation of Selenomethionyl PAPS Reductase. Selenomethionine-containing PAPS reductase was prepared as reported with modifications (*24*). Briefly, recombinant *E. coli* were grown in modified M9 minimal media (6.78 g/L Na_2HPO_4, 3.00 g/L KH_2PO_4, 0.50 g/L NaCl, 1.24 g/L $(NH_4)_2SO_4$, 2 mM $MgSO_4$, 0.1 mM $CaCl_2$, 4 g/L glucose, trace amount of $ZnSO_4$, $MnSO_4$, H_3BO_3, $NaMoO_4$, $CoCl_2$, KI, $CuSO_4$, $FeSO_4$, and H_2SO_4) (*25*) containing 100 μg/mL ampicillin at 37 °C until A_{600nm} reached 0.6−0.8. A sterile mixture of amino acids (100 mg/L L-lysine, L-phenylalanine, and L-threonine; 50 mg/L L-isoleucine, L-leucine, and L-valine; and 60 mg/L L-selenomethionine) was then added. Protein expression was induced 15 min later by addition of 0.1 mM IPTG and shaken at 15 °C for 12 h at 220 rpm. The procedures for purification were the same as described above.

Crystallization of Native and SeMet PAPS Reductase. Purified PAPS reductase was extensively dialyzed against Tris-HCl buffer (50 mM, pH 8.0) and concentrated to 10 mg/mL for crystallization using Amicon spin concentrators. Native protein was crystallized with the presence of 5 mM TCEP and 1 mM PAPS by hanging drop vapor diffusion using 2 μL drops of protein mixed with an equal volume of reservoir buffer (30% PEG 6000, 0.1 M HEPES, pH 7.0). After 3 weeks, the crystals grew to full size of about 0.25 mm × 0.2 mm × 0.15 mm. Diffraction of crystals improved significantly by soaking with DTT followed by PAP. Crystals were transferred and soaked in a buffer containing 32% PEG 6000, 0.1 M HEPES, pH 7.0, and 10 mM DTT for 30 min and then soaked in a buffer containing 32% PEG 6000, 0.1 M HEPES, pH 7.0, and 2 mM PAP for 10 min. The SeMet-modified protein crystals were grown by hanging drop against 30% PEG 6000 and 0.1 M HEPES, pH 7.0, and grew to about one-third the size of native crystals. All crystals were transferred to Paratone-N and flash frozen in a stream of nitrogen at 100 K for data collection.

Table 1: Data Collection, Phasing, and Refinement Statistics

	Se peak	Se remote	Se inflection	native PAP complex
X-ray source	SSRL BL 9-2	SSRL BL 9-2	SSRL BL 9-2	SSRL BL 9-2
wavelength (Å)	0.97879	0.91838	0.97931	0.97944
resolution (Å)	3.10 (3.21−3.10)	3.10 (3.21−3.10)	3.10 (3.21−3.10)	2.05 (2.10−2.05)
space group	$P2_12_12_1$			$P2_12_12_1$
cell parameters *a*, *b*, *c* (Å)	43.849, 68.651, 325.599			49.418, 63.082, 323.960
monomers/ASU	4			4
V_M (Å^3/Da), % solvent	2.09, 41.08			2.08, 40.8
no. of reflections	129139	129670	129271	266384
no. of unique	18686	18665	18680	62580
R_{merge}[a] (%)	6.6 (42.2)	6.2 (39.8)	6.9 (42.5)	7.3 (37.3)
mean $(I)/\sigma(I)$	21.8 (4.4)	24.9 (5.7)	22.2 (4.4)	7.2 (1.6)
completeness (%)	99.5 (99.6)	99.4 (99.6)	99.5 (99.0)	96.5 (78.2)
no. of Se sites	12			
figure of merit (solve/resolve)	0.57/0.71			
Refinement Statistics				
resolution (Å)				40−2.10
no. of reflections ($F \geq 0$)				55,322
R-factor[b]				19.3
R-free[b]				24.6
rms bond length (Å)				0.009
rms bond angles (deg)				1.178
Ramachandran Plot Statistics				
residues[c]				903
most favorable region (%)				89.5
allowed region (%)				9.6
generously allowed region (%)				0.9
disallowed (%)				0.0
Asymmetric Unit Content				
non-hydrogen protein atoms				8175
water				333
PAPs (atoms)				108

[a] $R_{merge} = \sum_h\sum_i|I_h - I_{hi}|/\sum_h\sum_i I_{hi}$, where I_h is the mean of I_{hi} observations of reflection *h*. Numbers in parentheses represent highest resolution shell. [b] *R*-factor and *R*-free $= \sum||F_o| - |F_c|| / \sum|F_o| \times 100$ for 95% of recorded data (*R*-factor) or 5% of data (*R*-free). [c] Number of non-proline and non-glycine residues used for calculation.

Data Collection and Phase Determination. X-ray data of two crystals (SeMet and DTT/PAP soaked native) were collected on beam line 9-2 at the Stanford Synchrotron Radiation Laboratory (SSRL). Both crystals belong to the space group $P2_12_12_1$ with slightly different cell parameters (Table 1). The Matthews coefficient V_M (*26*) was calculated to be 2.08 Å^3/Da assuming four monomers per asymmetric unit (ASU), which corresponds to a solvent content in the crystal of ~41%.

Multiwavelength anomalous dispersion (MAD) data were collected at three wavelengths corresponding to the selenium absorption edge (peak and inflection point) as well as a high-energy remote wavelength (Table 1). The three data sets were processed with DENZO and SCALEPACK (*27*). The 3.1 Å resolution data were input into the program SOLVE (*28*), which was able to locate all 12 selenium sites in the asymmetric unit. The overall figure of merit (FOM) from SOLVE was 0.57. The phases were improved by solvent flattening using the program RESOLVE (*29, 30*), which increased the FOM to 0.71 for all data to 3.1 Å resolution. An electron density map generated from RESOLVE contained features representing protein secondary structures, which was used to build an initial polyalanine model for four monomers in the asymmetric unit. A polyalanine backbone corresponding to residues 4−210 except 126−129 and 162−167 could not be traced. The four subunits in the ASU assembled into two homodimers.

The PAP complex X-ray diffraction yielded an anisotropic diffraction pattern. The diffraction along the *c*-axis went well beyond 2.0 Å resolution while the other two directions only diffracted to about 2.1 Å resolution. Therefore, the data were truncated at 2.05 Å resolution for all directions and processed. (Subsequent analysis revealed the elongated dimeric assembly for both dimers aligned along the *c*-axis generating more lattice contacts and tighter packing along the *c*-axis resulting in higher order along this axis.) The data set was indexed and integrated with MOSFLM and was reduced with SCALA in the CCP4 program suite (*31*). One SeMet-derived polyalanine dimer was used to solve the structure of the PAP complex by molecular replacement using the program PHASER (*32*). The molecular replacement search successfully produced a result structure with likelihood gain = 1805.8 containing two such dimers in each ASU.

Model Building and Refinement. Model building was done using the molecular graphics program COOT (*33*). Energy minimization-coupled coordinate and *B*-factor refinement were carried out with the program CNS (*34*) using 95% of the data while the remaining 5% data were left out and used as a reference to calculate *R*-free. During each stage of refinement, the *R*-free and *R*-factor decreased. The noncrystallographic symmetry was tightly constrained at first and gradually reduced, resulting in both the *R*-factor and *R*-free decreasing. The final steps of refinement were done with implementation of the TLS parametrization in the macromolecular refinement program REFMAC (*35*). The conventional *R*-factor fell to 19.3% and the corresponding *R*-free was 24.6%. The program PROCHECK (*36*) gave that 89.5% of the residues fall within the most favored region of a Ramachandran plot, and none of the residues were in the disallowed region.

RESULTS AND DISCUSSION

Crystallographic Properties. The final structural model contains four subunits of *Saccharomyces cerevisiae* PAPS reductase in the asymmetric unit that assemble into two homodimers packing along the *c*-axis of the crystal lattice. The polypeptide chains are designated as subunits A through D (two dimers correspond to subunits A-B and C-D). In the final model, the four subunits have an overall average *B*-factor of 36.7, 36.4, 36.4, and 37.1 Å^2, respectively, slightly higher than the Wilson plot *B*-value of 30.9 Å^2. Four PAP molecules were found bound to the active sites in the structure with an average *B*-factor of 31.9 Å^2. The C subunit is the most completely defined model because unambiguous electron density allowed the tracing of residues 1−257 of the 261 possible residues. Residues 238−242, 238−244, and 238−243 in the A, B, and D subunits, respectively, are disordered. This residue stretch corresponds to a small loop that precedes the C-terminal active site Cys245. The C-terminal tail containing the highly conserved active site sequence ^{244}ECGIH^{248} is observed in all four monomers in the asymmetric unit with the exception of Glu244 of the B subunit, which is disordered. The ECGIH motif has an elevated average *B*-factor of 46.9 Å^2, compared to the average *B*-factor for the protein (36.7 Å^2), which indicates the higher flexibility of this part of the protein.

Subunit Structure. As shown in Figure 1A, each of the *S. cerevisiae* PAPS reductase peptide chains folds into a single domain consisting of a central six-stranded β-sheet surrounded by α-helices. The protein adopts a Rossmann-like nucleotide-binding fold (*37*) with a central six-stranded β-sheet, except β-strands 5 and 6 are topologically swapped and β-strand 5 runs antiparallel to the other five strands. (Secondary structure nomenclature is adopted from the homologous *E. coli* structure (*13*).) The first 13 residues of each subunit fold into a β-hairpin structure separated from the central β-sheet, which is a unique feature not seen in other known APS/PAPS reductase structures. In *E. coli* PAPS reductase, this N-terminal stretch adopts a different conformation by forming two short helices (Figure 2A). The first 26 residues in *P. aeruginosa* APS reductase are disordered but appear to adopt a different disposition based on the first residues observed in the structure (*12*). This β-hairpin in yeast PAPS reductase appears to play an important functional role because it is involved in forming dimerization interactions.

The active site is located at the C-terminal end of strands β1 and β4 where the product PAP was found to bind (Figure 1A). The 3′-phosphate of PAP is accommodated by a modified P-loop or "pyrophosphate-binding" loop (PP-loop) (*38*). Additional features that also shape the active site include the Arg loop (residues 159−167) between β4 and β5 and the Ω-loop (residues 213−226) (*39*). The C-terminal tail of the enzyme, which contains the conserved ^{244}ECGIH^{248} sequence, forms a loop over helix α8 and extends over the bound PAP in the center of the six-stranded β-sheet and contacts helix α7.

Quaternary Structure. The molecular mass of recombinant *S. cerevisiae* PAPS reductase in solution was determined by size-exclusion chromotagraphy to be ~75 kDa, indicating a homodimer (*40*). In the crystal, four subunits in the asymmetric unit assemble into two biological dimers. The dimerization interactions are mediated primarily through the

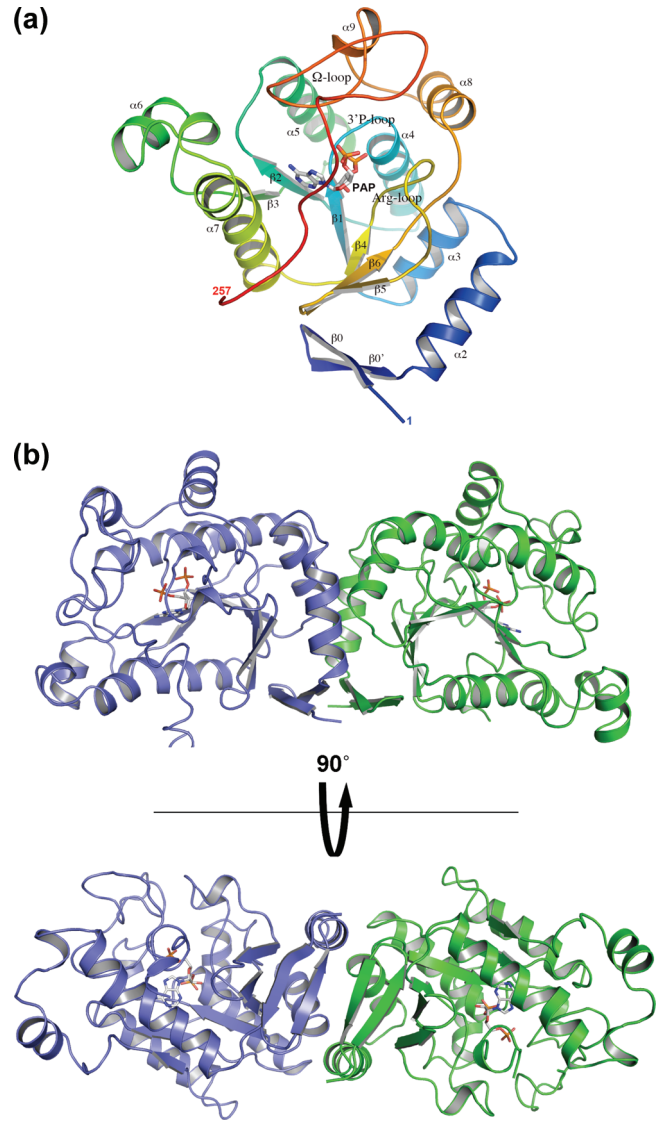

FIGURE 1: Structure of yeast PAPS reductase. (A) Ribbon diagram of the yeast PAPS reductase monomer. The polypeptide chain folds into a single domain and is colored in rainbow, from blue (N-terminus) to red (C-terminus). The secondary structure nomenclature is adopted from the *E. coli* PAPS reductase (*13*) (PDB: 1SUR) except strands β0 and β0′, which are unique for the yeast enzyme. The bound PAP molecule is shown in stick rendering revealing the active site. Active site loops are also labeled. (B) Ribbon diagram of the yeast PAPS reductase dimer. The two subunits are colored in blue and green, respectively. Two monomers pack against each other through helices α2 and α3. The N-terminal β-hairpins, although in close proximity, do not form a contiguous four-strand β-sheet; rather water molecules (not shown) mediate contacts across the 2-fold. Total surface area buried upon dimer formation is 2290 Å^2. All protein structure figures were generated using the program PyMol (http://www.pymol.org).

N-terminal regions of each subunit, including the N-terminal β-hairpins, helices α2 and α3, and the loop connecting α4 and β2 (Figure 1B). The N-terminal β-hairpins align in an antiparallel arrangement across the dimer 2-fold. However, the two β0′ strands are too far from the dimer 2-fold to form direct main chain hydrogen-bonding interaction that would result in a contiguous four-stranded antiparallel β-sheet across the dimer axis (Figure 1B). Instead, the two β0′ strands contact each other through water-mediated hydrogen bonds and van der Waals stacking interaction between residues Leu10 and Thr13. Additionally, residues in the center of helices

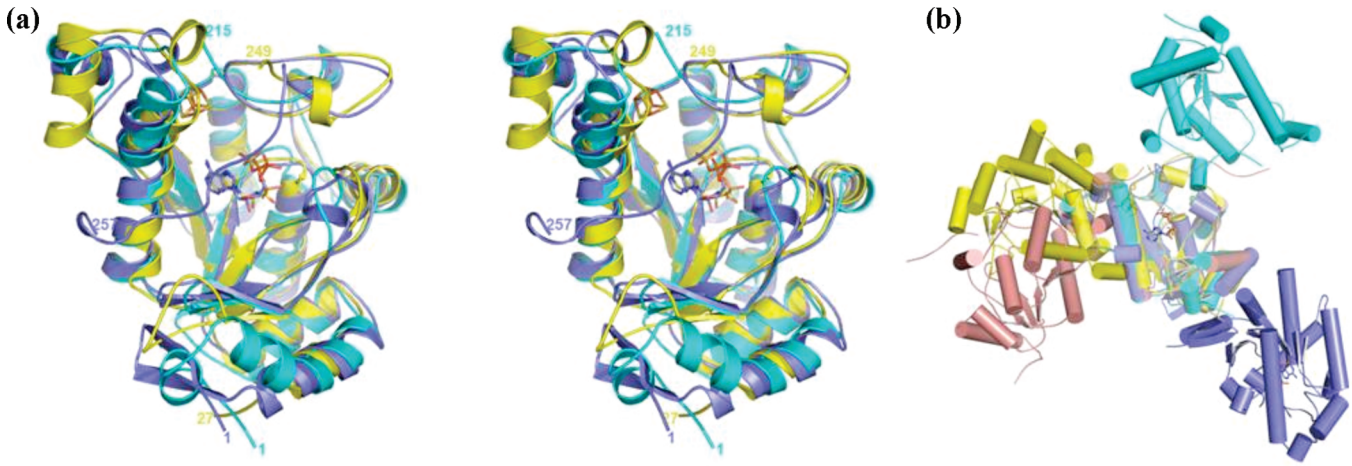

FIGURE 2: Comparison of PAPS/APS structures. (a) Stereoview showing the superposition of monomers from yeast PAPS reductase (blue), apo *E. coli* PAPS reductase (marine), and *P. aeruginosa* APS reductase (yellow). The PAP bound in the yeast structure is shown in sticks with blue-colored carbon atoms. The bound APS and [4Fe-4S] as seen in *P. aeruginosa* APS reductase are also displayed as sticks. The first and last residues observed in each structure are numbered in their respective color. Note the similarity of overall folds but the difference in the N-termini secondary structure. (b) Comparison of the different APS and PAPS reductase dimeric assemblies. Dimers of yeast PAPS reductase (blue), *E. coli* PAPS reductase apo (marine), *E. coli* PAPS reductase (pink) as seen bound to thioredoxin, and *P. aeruginosa* APS reductase (yellow) are shown in superimposition based on a constant monomer shown in transparent color in the center. The substrates (APS and PAP) and [4Fe-4S] center are displayed in stick rendering.

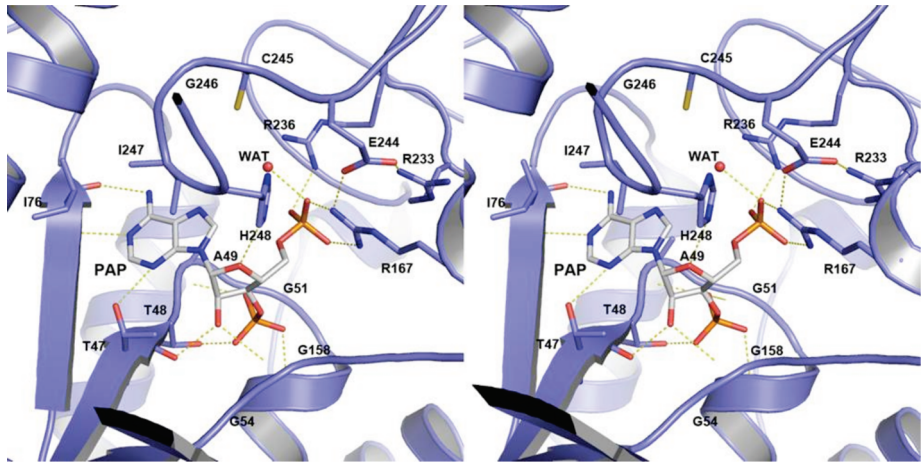

FIGURE 3: Active site of yeast PAPS reductase. The stereoview of the C-subunit PAPS reductase active site shows the bound PAP molecule as a stick model. The substrate is recognized by residues from highly conserved motifs, including the 3′-P loop (^{51}GLTG^{54}), Arg loop (^{161}KSQGSARSQLS^{171}), DT motif (^{76}IDTL^{79}), and the C-terminal ECG(I/L)H motif. The bound substrate and two arginine residues recruit the C-terminal catalytic motif ECGIH into the active site. At the sulfate binding site, a water molecule occupies the space between Cys245, His248, and bound substrate forming two hydrogen bonds to both His248 and the 5′-phosphate of PAP.

α2 and α3 (Trp20, Leu27, Trp36, Val39, Thr40, and Pro42) form a hydrophobic patch with their dimeric 2-fold related residues. The protein dimer is further stabilized by hydrogen bonds between Glu15 and dimeric related His43, between His19 and main chain carbonyl of Ile18, and between Lys26 and main chain carbonyl of Lys67. The combined dimeric interactions result in a total buried surface area of 2290 Å^2 (*34*).

The dimeric assembly of yeast PAPS reductase seen here differs radically from both of the dimeric assemblies of the *E. coli* PAPS reductase (*13, 16*), the tetrameric *Pseudomonas* APS reductase (*12*) (Figure 2B), and the monomeric *M. tuberculosis* APS reductase (*14*). The unique N-terminal β-hairpin in the yeast PAPS reductase appears to help trigger a different assembly involving the β-hairpin and helices α2 and α3. These results suggest that the divergent quaternary assemblies found among these enzymes from different species appear to have little consequence on sulfate reduction activity.

Substrate Recognition. PAP is bound to all four subunits in the asymmetric unit. The core of the protein forms a deep active site pocket with PAP sitting in the center, and the C-terminal loop acts as a lid covering the active site to enclose the substrate. The substrate is recognized by conserved motifs. The interactions between PAP and the enzyme are shown in Figure 3. The adenine ring of PAP makes three hydrogen bonds with Ile76 and Thr47. N1 and N6 of the adenine ring each make a hydrogen bond to Ile76 main chain atoms N and C, respectively. The Oγ1 atom of Thr47 hydrogen bonds to N3 of the adenine ring. Ile76 immediately precedes the conserved DT motif, which was proposed to be a sulfate-binding motif (*38*). However, in the structure present here, Asp77 and Thr78 do not interact with PAP and are too far away to interact with a sulfate group in PAPS (Figure 3). The same conformation is also observed in the *Pseudomonas* APS reductase structure (*12*).

Threonine 47 initiates a conserved motif (^{47}TTAFGLTG^{54}) that is observed in many APS/PAPS reductases. This was

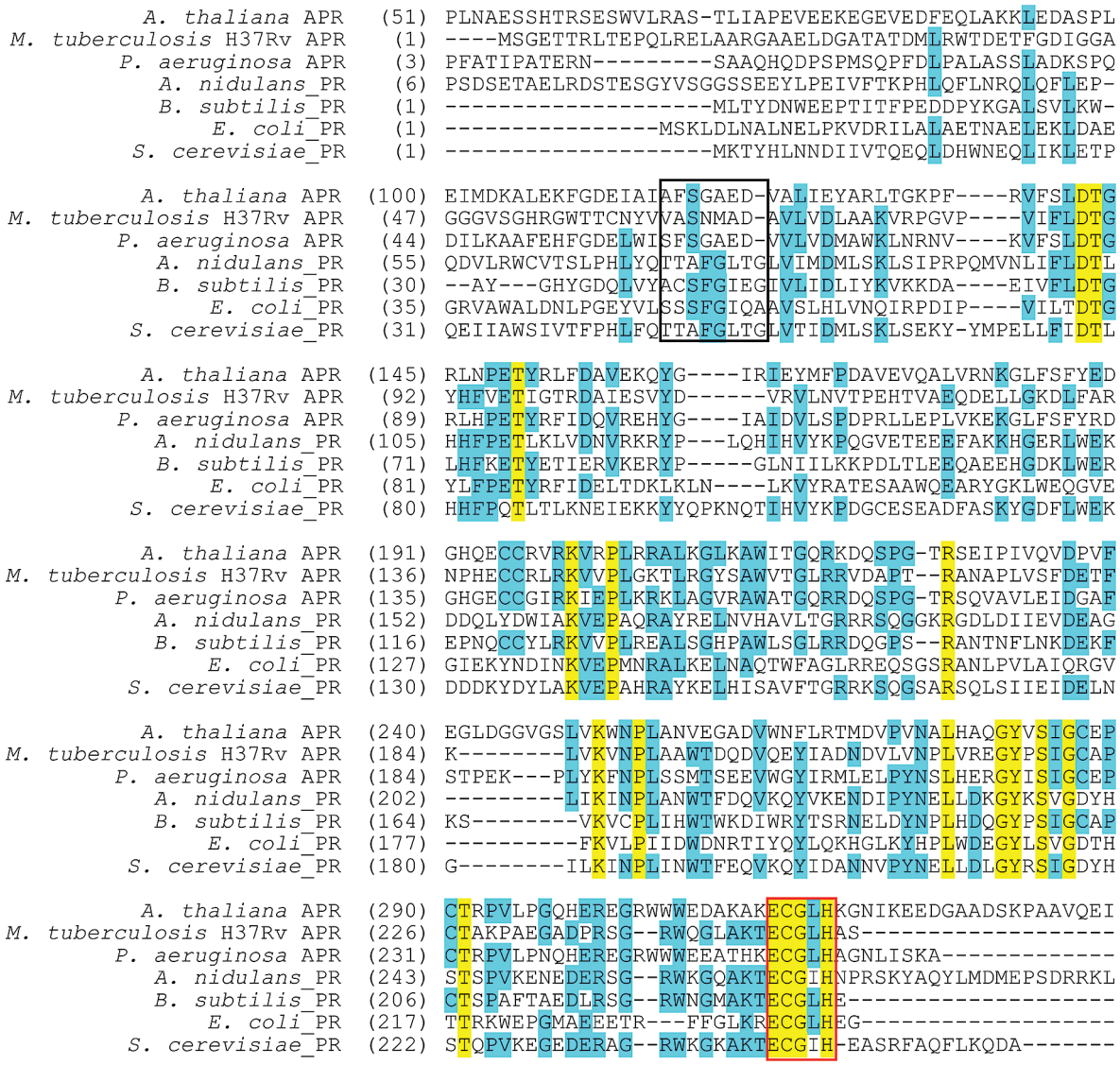

FIGURE 4: Sequence alignment of APS reductases from *A. thaliana*, *M. tuberculosis H37Rv*, *P. aeruginosa*, and PAPS reductases from *A. nidulans*, *B. subtilis*, *E. coli*, and *S. cerevisiae*. The alignment was generated using AlignX in the VectorNTI suite (Invitrogen). The black box outlines the putative 3′-P loop, which in the yeast PAPS reductase structure here is involved in binding the adenine ring and 3′-phosphate of PAPS. The red box outlines the conserved catalytic C-terminal loop containing the Cys245-His248 catalytic dyad.

originally identified as a potential pyrophosphate-binding loop (PP-loop) based on its conservation in many enzymes that cleave the $\alpha-\beta$ phosphodiester bond (*38*). This PP-loop was assumed to bind the 5′-phosphosulfate moiety of APS/PAPS in the reductases. However, in PAPS reductase, the loop is actually involved in defining the 3′-phosphate binding pocket. The 3′-phosphate oxygens hydrogen bond to main chain amide nitrogens in residues Ala49, Gly51, and Gly54 (Figure 3). Additionally, Oγ1 of Thr48 is also in hydrogen-bonding distance to a 3′-phosphate oxygen.

In the APS reductase, which binds APS without a 3′-phosphate, positions equivalent to Thr53 and Gly54 (yeast PAPS reductase) are typically Glu and Asp (Figure 4). As observed in the *Pseudomonas* APS reductase structure, the carboxylate group of Asp66 (equivalent to yeast Gly54) occupies a similar position to the PAPS 3′-phosphate, with Glu65 nearby (*12*) (Figure 5A). Thus, negatively charged residues in these positions likely discriminate between reducing APS over PAPS for enzyme specificity. In the *Bacillus subtilis* enzyme, which has been reported to reduce both APS and PAPS but with higher efficiency toward PAPS (*41*), these residues are Glu-Gly (Figure 4). The conformation of this 3′-phosphate binding loop in the *E. coli* PAPS reductase structures is in a more open conformation compared to the yeast PAPS reductase structure here and the *Pseudomonas* APS reductase structure. This is possibly because both of the *E. coli* structures do not contain bound nucleotide (Figure 5A) (*13, 16*) and suggests this 3′-phosphate binding loop might be flexible and move upon substrate binding and product release. Another indicator of the plasticity of this loop is the conservation of glycine residues and in both PAPS and APS reductase. Additionally, the 3′-P loop also contains a deletion of one residue in most APS reductases, including the *Pseudomonas* enzyme.

A number of positively charged residues are in the vicinity of the 5′-phosphate of the bound PAP including Lys139, Arg167, Arg233, Arg236, and His248. With the exception of Arg167 and His248, all of these basic residues can be found in the *Pseudomonas* APS reductase structure interacting with the 5′-phosphosulfate moiety of APS (Figure 5B). In yeast PAPS reductase, Arg167 and Arg236 interact with the 5′-phosphate of PAP, while Lys139, Arg233, and His248

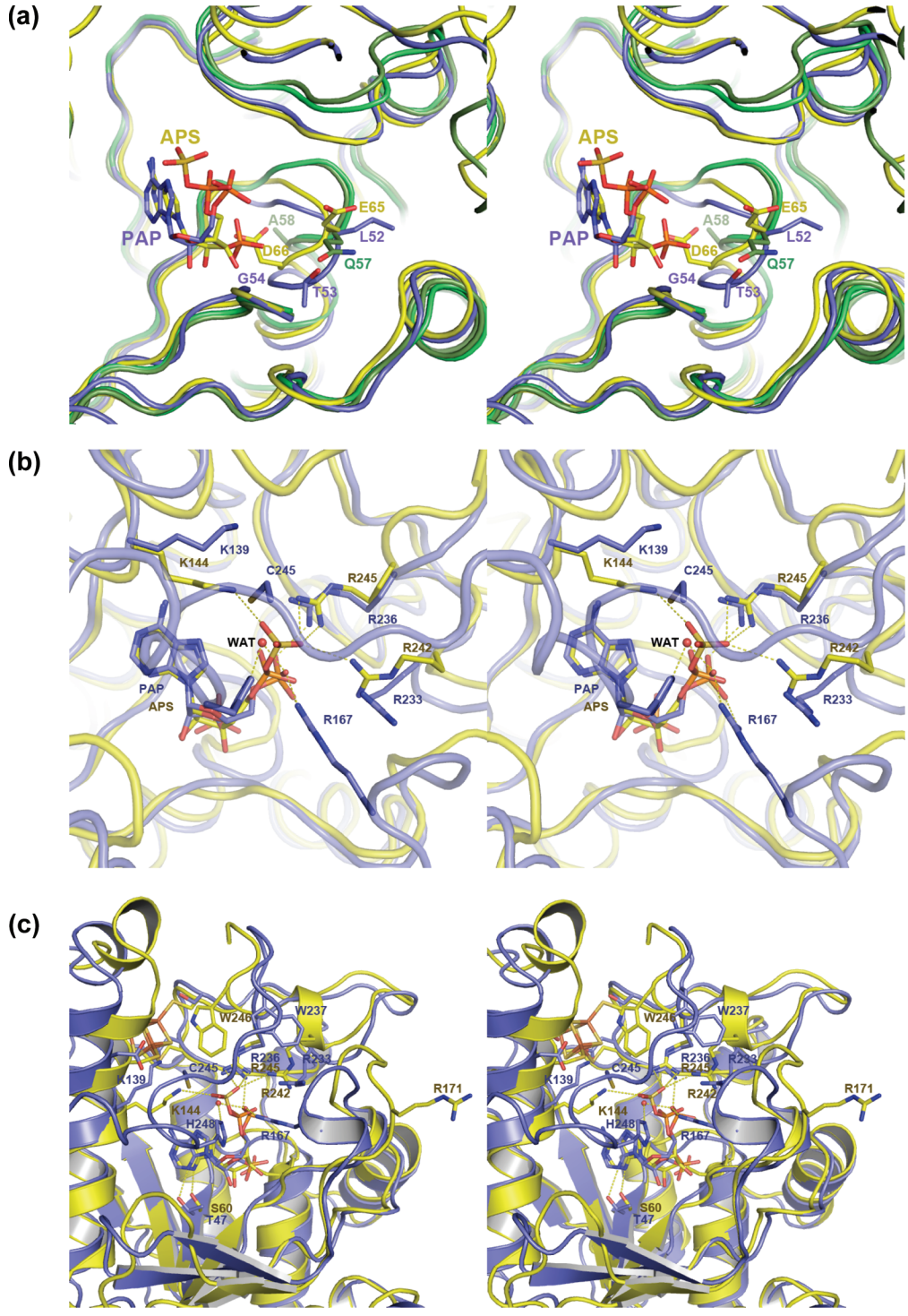

FIGURE 5: Comparison of APS/PAPS reductase active sites. (A) Comparison of the 3′-phosphate binding loop. Stereoview superposition of the active sites of all the APS/PAPS reductase structures currently known. The 3′-phosphate binding loop for *E. coli* PAPS reductase in both the ligand-free apo form (light green) and bound to thioredoxin (dark green) is in a more "open" conformation compared to yeast PAPS reductase (blue) and *Pseudomonas* APS reductase (yellow). The highly conserved dyad sequence of Glu65-Asp66 in APS reductase is shown in yellow stick side chains. Asp66 would occlude 3′-phosphate binding of PAPS, thus explaining the enzyme's preference for APS. The equivalent residues in the PAPS reductases of yeast and *E. coli* are also shown in their respective colors. In yeast PAPS reductase, Thr53-Gly54 is the equivalent dyad sequence, but Leu52 is structurally equivalent to Glu65 of APS reductase. The C-terminal loop in yeast PAPS reductase is omitted for clarity. (B) Detailed stereoview superposition of yeast PAPS reductase (blue) onto *Pseudomonas* APS reductase (yellow) displayed with the respective PAP and APS ligands bound. Residues that interact with the 5′-phosphosulfate moiety are shown in stick with respective coloring. A water molecule is observed to occupy the position of sulfate in the yeast PAP structure. Also shown is the ordered C-terminal tail from yeast PAPS reductase containing active site residues Cys245 and His248. (C) Wide-angle stereoview superposition of yeast PAPS reductase (blue) onto *Pseudomonas* APS reductase (yellow) displayed with the respective PAP and APS ligands bound. Shown is the [4Fe-4S] center in *Pseudomonas* APS reductase but absent in PAPS reductase. Also shown is the comparison in dispositions of conserved Arg167 of the Arg loop. In yeast, Arg167 points toward the 5′-phosphate of PAP, but in *Pseudomonas*, Arg171 swings 18 Å to point to bulk solvent.

would likely interact with the sulfate moiety of PAPS. Highly conserved His248 is part of the active site C-terminal tail and was disordered in all previous PAPS/APS reductase structures. In this structure here, His248 is close enough to interact with a β-sulfate of PAPS as well as play an important role in catalysis (see below).

It is interesting to note that Arg167, which is part of a conserved Arg loop, is seen here interacting with the 5′-phosphate of PAP. This conformation is similar to that seen in the *E. coli* PAPS reductase structure determined in the absence of substrate. However, in *Pseudomonas* APS reductase, this arginine swings ~18 Å out of the active site where it points to bulk solvent (Figure 5C). In fact, none of the residues of the conserved Arg loop in *Pseudomonas* APS reductase are observed to interact with the APS substrate. In the crystal structure of the *E. coli* PAPS reductase structure trapped in the thioredoxin-bound intermediate, the equivalent arginine is also seen pointing out to bulk solvent. These data suggest that the Arg loop flexibility may be important for catalytic turnover, possibly assisting in releasing the E-Cys-thiosulfonate intermediate out of the active site pocket where it can interact with thioredoxin to be reduced.

In APS reductases, the iron−sulfur center is important in the catalysis (*10, 17, 18*), but its absence in PAPS reductase questions its functional role as an electron carrier (*12, 14, 17, 19*). In *Pseudomonas* APS reductase, the iron−sulfur center is fastened between a helix and a loop where it is coordinated by four cysteine residues (*Pseudomonas* numbering): Cys139 and Cys140 of helix α7 and Cys228 and Cys231 in the Ω-loop between helix α9 and the C-terminus (Figure 5C). In yeast PAPS reductase, the cysteine residues have changed to Tyr134, Asp135, Asp219, and Ser222. However, the overall structure of helix α7 and the Ω-loop are very similar in both structures (Figures 2A and 5C), although the bend in helix α7 is less pronounced in PAPS reductase because of the absence of the [4Fe-4S] center. Given the absence of the [4Fe-4S] cluster in PAPS reductase, the role of the cluster in APS reductase may be to help adjust the reduction potential of the active site cysteine.

The C-Terminal ECGIH Motif. The *S. cerevisiae* PAPS reductase structure reveals for the first time the structure of the C-terminal region containing the conserved catalytic ^{244}ECGIH^{248} motif, which includes Cys245 that forms the thiosulfonate intermediate, which is subsequently reduced by thioredoxin. The C-terminal tail stretches from above helix α8 and runs along the protein surface over the active site across to helix α7 where Phe253, Phe256, and Leu257 of the C-terminus pack against a hydrophobic patch on helix α7 (Figure 1A). These hydrophobic residues in yeast PAPS reductase are not conserved in other organisms. Sequence analysis has shown that only *Aspergillus nidulans* PAPS reductase has the sequence KYAQYL homologous to ^{252}RF-AQFL^{257} from *S. cerevisiae* PAPS reductase (Figure 4). In other sulfate reductases, these residues are either truncated or continue into a thioredoxin-like domain as seen in APS reductases from plants (*42*) and green algae (*43*).

The presence of this hydrophobic anchor at the end of the C-terminus suggests that the tail may not swing completely off the protein as seen in *E. coli* PAPS reductase (*16*). Furthermore, residues immediately preceding the conserved ^{244}ECGIH^{248} sequence are disordered in three of the four subunits and contain high *B*-values in the fourth subunit where they can be modeled. This suggests that the active site loop may be anchored at both ends and only the loop-center, containing the enzyme-thiosulfonate intermediate (Cys245-S-SO_3^-), flips out of the active site to interact with thioredoxin for reduction. This may be a feature limited to yeast, and possibly *A. nidulans*, PAPS reductase because of the unique hydrophobic C-terminal tail. However, we cannot rule out that a few weak crystal lattice contacts may also help to tether the C-terminal tail allowing for its ordered observance. The region centered around Ser251 of all four subunits in the asymmetric unit makes van der Waals contacts with crystal-packing subunits.

Future experiments are needed to test the mobility of the C-terminal tail. If the C-terminal tail is not completely released from the yeast PAPS reductase enzyme, thioredoxin may interact with different surface residues compared to those observed in the *E. coli* complex structure (*16*). Mutations at the end of helix α7, the Arg loop, and the Ω-loop may affect thioredoxin binding and turnover because they are in close proximity of the center of the loop.

The conserved sequence ^{244}ECGIH^{248} forms a single helical turn directly above the bound substrate (Figure 3). Rather than being a part of the substrate recognition, the ^{244}ECGIH^{248} motif seems to be recruited to the active site through interactions with PAP and other active site residues. Glu244 forms salt linkages with Arg167 and Arg233, two basic residues that interact with phosphosulfate moiety of PAPS. The hydrophobic side chain of Ile247 packs against the adenine ring of the substrate where the other side of the ring stacks against the peptide bond between Thr48 and Ala49 of the 3′-phosphate binding loop. These interactions keep the catalytic Cys245 in close proximity to the potential sulfate of PAPS. Cys245 is 5.8 Å away from a 5′-phosphate oxygen of PAP or 3.5 Å away from the sulfur of a superimposed APS molecule (Figure 5). This conformation of Cys245 is ideally suited for an in-line attack on the β-sulfate of PAPS. The presence of Gly246 provides extra flexibility to permit the loop to bend toward the substrate. The turn at Gly246 also brings His248 directly above O4′ of the ribose ring, where it is in hydrogen-bonding distance. The side chain of His248 is also 4.2 Å from the Sγ of Cys245 and may serve as a catalytic base to deprotonate the active site cysteine. Figure 5B shows a possible sulfate placement based on the superposition of APS binding from the *Pseudomonas* APS reductase structure. However, this superposition is based on protein and not substrate; nevertheless, it is conceivable that upon PAPS binding the sulfate would not intervene between His248 and Cys 245 and a small movement in either residue would bring the imidazole group closer to Cys245. Alternatively, His248 may also serve to help position the sulfate moiety by hydrogen bonding to the sulfate, thus holding it for an in-line attack by Cys246. This histidine is conserved in all PAPS reductases and all but a couple APS reductase genes. However, in the genera *Chloroflexus* and *Deinococcus*, where His is changed to Trp, the bacteria were first isolated from thermal hot springs which supply a natural source of reduced sulfur (*44, 45*), possibly making a functional APS reductase unnecessary for growth. Only the APS reductase gene found in *Cytophaga hutchinsonii* has Asn substituted for His, but functional APS reductase activity has yet to be proven for the gene product. Experiments are underway to resolve the exact role of His248.

Concluding Remarks. The crystal structure presented here of the *S. cerevisiae* PAPS reductase-PAP complex likely represents the conformation of the PAPS-bound state prior to the formation of the covalent intermediate. Crystals were grown with PAPS present, which should generate the enzyme-thiosulfonate intermediate (Cys245-S-SO_3^-) with PAP product. However, these crystals diffracted poorly, suggesting a partial disorder. The crystals were soaked with DTT in attempts to reduce the enzyme-thiosulfonate intermediate and possibly produce a more ordered C-terminus. While DTT was not successful in reducing the thiosulfonate intermediate in APS reductase (except when unfolded) (*12, 14*), we found DTT to be an effective reducing agent for yeast PAPS reductase and support multiple turnovers under native conditions (Supporting Information). Soaking the PAPS reductase crystals in 10 mM DTT for 30 min and subsequently with additional PAP improved the X-ray diffraction to 2.05 Å resolution. The electron density map showed no sign of a sulfonate group around Cys245, but excess PAP was able to bind to the active site. The reduction of the Cys245-S-SO_3^- intermediate likely resulted in the ordering of the C-terminal tail containing the ECG(I/L)H motif, which hitherto has never been observed in a APS/PAPS reductase structure bound to the active site.

The previous structure of *P. aeruginosa* APS reductase was grown with APS, which was not reduced, resulting in disorder of the C-terminal tail with the covalently bound Cys-thiosulfonate intermediate; nevertheless, excess APS was seen in the active site pocket (*12*). The C-terminal ECG(I/L)H motif of the *E. coli* PAPS reductase was seen in the trapped intermediate bound the thioredoxin (*16*), but the motif binds in an extended conformation against the surface of the thioredoxin. While this structure was pivotal in better understanding the complete mechanism of sulfate reduction, it did not show how the conserved C-terminal motif in the APS/PAPS reductases bound to the active site or reveal the functional roles of other residues in this motif. The crystal structure of yeast PAPS reductase presented here has provided additional structural detail for further understanding the sulfate reduction pathway. The C-terminal ECGIH motif observed here provides key information of the active site for all sulfate-reducing enzymes and indicates a possible Cys-His catalytic dyad in sulfate reduction.

ACKNOWLEDGMENT

Portions of this research were carried out at the Stanford Synchrotron Radiation Laboratory, a national user facility operated by Stanford University on behalf of the U.S. Department of Energy, Office of Basic Energy Sciences. The SSRL Structural Molecular Biology Program is supported by the Department of Energy, Office of Biological and Environmental Research, and by the National Institutes of Health, National Center for Research Resources, Biomedical Technology Program, and the National Institute of General Medical Sciences.

SUPPORTING INFORMATION AVAILABLE

Detailed methods and results are given for using DTT as a surrogate small-molecule reducing agent to reduce the enzyme thiosulfonate intermediate. This material is available free of charge via the Internet at http://pubs.acs.org.

REFERENCES

1. Rabeh, W. M., and Cook, P. F. (2004) Structure and mechanism of O-acetylserine sulfhydrylase. *J. Biol. Chem. 279*, 26803–26806.
2. Thauer, R., Jungermann, K., and Decker, K. (1977) Energy conservation in chemotrophic anaerobic bacteria. *Bacteriol. Rev. 41*, 100–180.
3. Osslund, T., Chandler, C., and Segel, I. H. (1982) ATP sulfurylase from higher plants: Purification and preliminary kinetics studies on the cabbage leaf enzyme. *Plant Physiol. 70*, 39–45.
4. Seubert, P. A., Hoang, L., Renosto, F., and Segel, I. H. (1983) ATP sulfurylase from *Penicillium chrysogenum*: Measurements of the true specific activity of an enzyme subject to potent product inhibition and a reassessment of the kinetic mechanism. *Arch. Biochem. Biophys. 225*, 679–691.
5. Renosto, F., Seubert, P. A., and Segel, I. H. (1984) Adenosine 5′-phosphosulfate kinase from *Penicillium chrysogenum*. Purification and kinetic characterization. *J. Biol. Chem. 259*, 2113–2123.
6. Segel, I. H., Renosto, F., and Seubert, P. A. (1987) Sulfate-activating enzymes. *Methods Enzymol. 143*, 334–349.
7. Robbins, P. W., and Lipmann, F. (1958) Enzymatic synthesis of adenosine-5′-phosphosulfate. *J. Biol. Chem. 233*, 686–690.
8. Abola, A. P., Willits, M. G., Wang, R. C., and Long, S. R. (1999) Reduction of adenosine-5′-phosphosulfate instead of 3′-phosphoadenosine-5′-phosphosulfate in cysteine biosynthesis by *Rhizobium meliloti* and other members of the family Rhizobiaceae. *J. Bacteriol. 181*, 5280–5287.
9. Williams, S. J., Senaratne, R. H., Mougous, J. D., Riley, L. W., and Bertozzi, C. R. (2002) 5′-adenosinephosphosulfate lies at a metabolic branch point in mycobacteria. *J. Biol. Chem. 277*, 32606–32615.
10. Kopriva, S., Buchert, T., Fritz, G., Suter, M., Benda, R., Schunemann, V., Koprivova, A., Schurmann, P., Trautwein, A., Kroneck, P., and Brunold, C. (2002) The presence of an iron-sulfur cluster in adenosine 5′-phosphosulfate reductase separates organisms utilizing adenosine 5′-phosphosulfate and phosphoadenosine 5′-phosphosulfate for sulfate assimilation. *J. Biol. Chem. 277*, 21786–21791.
11. Peck, H. D. (1961) Enzymatic basis for assimilatory and dissimilatory sulfate reduction. *J. Bacteriol. 82*, 933–939.
12. Chartron, J., Carroll, K., Shiau, C., Gao, H., Leary, J., Bertozzi, C., and Stout, C. (2006) Substrate recognition, protein dynamics, and iron-sulfur cluster in *Pseudomonas aeruginosa* adenosine 5′-phosphosulfate reductase. *J. Mol. Biol. 364*, 152–169.
13. Savage, H., Montoya, G., Svensson, C., Schwenn, J. D., and Sinning, I. (1997) Crystal structure of phophoadenylyl sulphate (PAPS) reductase: a new family of adenine nucleotide a hydrolases. *Structure 5*, 895–906.
14. Carroll, K., Gao, H., Chen, H., Stout, C., Leary, J., and Bertozzi, C. (2005) A conserved mechanism for sulfonucleotide reduction. *PLoS Biol. 3*, e250.
15. Weber, M., Suter, M., Brunold, C., and Kopriva, S. (2000) Sulfate assimilation in higher plants characterization of a stable intermediate in the adenosine 5′-phosphosulfate reductase reaction. *Eur. J. Biochem. 267*, 3647–3653.
16. Chartron, J., Shiau, C., Stout, C., and Carroll, K. (2007) 3′-Phosphoadenosine-5′-phosphosulfate reductase in complex with thioredoxin: A structural snapshot in the catalytic cycle. *Biochemistry 46*, 3942–3951.
17. Carroll, K., Gao, H., Chen, H., Leary, J., and Bertozzi, C. (2005) Investigation of the iron-sulfur cluster in *Mycobacterium tuberculosis* APS reductase: Implications for substrate binding and catalysis. *Biochemistry 44*, 14647–14657.
18. Kim, S., Rahman, A., Bick, J., Conover, R., Johnson, M., Mason, J., Hirasawa, M., Leustek, T., and Knaff, D. (2004) Properties of the cysteine residues and iron-sulfur cluster of the assimilatory 5′-adenylyl sulfate reductase from *Pseudomonas aeruginosa*. *Biochemistry 43*, 13478–13486.
19. Kim, S. K., Rahman, A., Mason, J. T., Hirasawa, M., Conover, R. C., Johnson, M. K., Miginiac-Maslow, M., Keryer, E., Knaff, D. B., and Leustek, T. (2005) The interaction of 5′-adenylylsulfate reductase from *Pseudomonas aeruginosa* with its substrates. *Biochim. Biophys. Acta 1710*, 103–112.
20. Fritz, G., Buchert, T., Huber, H., Stetter, K., and Kroneck, P. (2000) Adenylylsulfate reductases from archaea and bacteria are 1:1 alphabeta-heterodimeric iron-sulfur flavoenzymes—high similarity of molecular properties emphasizes their central role in sulfur metabolism. *FEBS Lett. 473*, 63–66.

21. Meyer, B., and Kuever, J. (2008) Homology modeling of dissimilatory APS reductases (AprBA) of sulfur-oxidizing and sulfate-reducing prokaryotes. *PLoS ONE 3*, e1514.
22. Schiffer, A., Fritz, G., Kroneck, P., and Ermler, U. (2006) Reaction mechanism of the iron-sulfur flavoenzyme adenosine-5′-phosphosulfate reductase based on the structural characterization of different enzymatic states. *Biochemistry 45*, 2960–2967.
23. Sassetti, C., Boyd, D., and Rubin, E. (2001) Comprehensive identification of conditionally essential genes in mycobacteria. *Proc. Natl. Acad. Sci. U.S.A. 98*, 12712–12717.
24. Doublié, S. (1997) Preparation of selenomethionyl proteins for phase determination, in *Methods in Enzymology* (Carter, C. W., Jr., and Sweet, R. M., Eds.) pp 523−530, Academic Press, New York.
25. Sambrook, J., and Russell, D. W. (2001) *Molecular cloning: a laboratory manual*, 3rd ed., Cold Spring Harbor Laboratory Press, Cold Spring Harbor, NY.
26. Matthews, B. W. (1968) Solvent content of protein crystals. *J. Mol. Biol. 33*, 491–497.
27. Otwinowski, Z., and Minor, W. (1997) Processing of X-ray diffraction data collected in oscillation mode, in *Methods in Enzymology* (Carter, C. W., Jr., and Sweet, R. M., Eds.) pp 307−326, Academic Press, New York.
28. Terwilliger, T. C., and Berendzen, J. (1999) Automated structure solution for MIR and MAD. *Acta Crystallogr. D55*, 849–861.
29. Terwilliger, T. C. (1999) Reciprocal-space solvent flattening. *Acta Crystallogr. D55*, 1863–1871.
30. Terwilliger, T. C. (2000) Maximum likelihood density modification. *Acta Crystallogr. D56*, 965–972.
31. CCP4 (1994) The CCP4 suite: Programs for protein crystallography, *Acta Crystallogr. D50*, 760−763.
32. McCoy, A. J., Grosse-Kunstleve, R. W., Storoni, L. C., and Read, R. J. (2005) Likelihood-enhanced fast translation functions. *Acta Crystallogr., Sect. D: Biol. Crystallogr. 61*, 458–464.
33. Emsley, P., and Cowtan, K. (2004) Coot: model-building tools for molecular graphics. *Acta Crystallogr., Sect. D: Biol. Crystallogr. 60*, 2126–2132.
34. Brünger, A., Adams, P., Clore, G., DeLano, W., Gros, P., Grosse-Kunstleve, R., Jiang, J., Kuszewski, J., Nilges, M., Pannu, N., Read, R., Rice, L., Simonson, T., and Warren, G. (1998) Crystallography & NMR system: A new software suite for macromolecular structure determination. *Acta Crystallogr., Sect. D: Biol. Crystallogr. 54*, 905–921.
35. Winn, M. D., Isupov, M. N., and Murshudov, G. N. (2001) Use of TLS parameters to model anisotropic displacements in macromolecular refinement. *Acta Crystallogr., Sect. D: Biol. Crystallogr. 57*, 122–133.
36. Laskowski, R. A., MacArthur, M. W., Moss, D. S., and Thornton, J. M. (1993) PROCHECK: a program to check the stereochemical quality of protein structures. *J. Appl. Crystallogr. 26*, 283–291.
37. Rossmann, M. G., Moras, D., and Olsen, K. W. (1974) Chemical and biological evolution of nucleotide-binding protein. *Nature 250*, 194–199.
38. Bork, P., and Koonin, E. (1994) A P-loop-like motif in a widespread ATP pyrophosphatase domain: implications for the evolution of sequence motifs and enzyme activity. *Proteins 20*, 347–355.
39. Leszczynski, J. F., and Rose, G. D. (1986) Loops in globular proteins: A novel category of secondary structure. *Science 234*, 849–855.
40. Schwenn, J. D., Krone, F. A., and Husmann, K. (1988) Yeast PAPS reductase: Properties and requirements of the purified enzyme. *Arch. Microbiol. 150*, 313–319.
41. Berndt, C., Lillig, C., Wollenberg, M., Bill, E., Mansilla, M., de Mendoza, D., Seidler, A., and Schwenn, J. (2004) Characterization and reconstitution of a 4Fe-4S adenylyl sulfate/phosphoadenylyl sulfate reductase from *Bacillus subtilis*. *J. Biol. Chem. 279*, 7850–7855.
42. Gutierrez-Marcos, J. F., Roberts, M. A., Campbell, E. I., and Wray, J. L. (1996) Three members of a novel small gene-family from *Arabidopsis thaliana* able to complement functionally an *Escherichia coli* mutant defective in PAPS reductase activity encode proteins with a thioredoxin-like domain and "APS reductase" activity. *Proc. Natl. Acad. Sci. U.S.A. 93*, 13377–13382.
43. Kim, S., Gomes, V., Gao, Y., Chandramouli, K., Johnson, M., Knaff, D., and Leustek, T. (2007) The two-domain structure of 5′-adenylylsulfate (APS) reductase from *Enteromorpha intestinalis* is a requirement for efficient APS reductase activity. *Biochemistry 46*, 591–601.
44. Pierson, B. K., and Castenholz, R. W. (1974) A phototrophic gliding filamentous bacterium of hot springs, *Chloroflexus aurantiacus*, gen. and sp. nov. *Arch. Microbiol. 100*, 5–24.
45. Ferreira, A. C., Nobre, M. F., Rainey, F. A., Silva, M. T., Wait, R., Burghardt, J., Chung, A. P., and da Costa, M. S. (1997) *Deinococcus geothermalis* sp. nov. and *Deinococcus murrayi* sp. nov., two extremely radiation-resistant and slightly thermophilic species from hot springs. *Int. J. Syst. Bacteriol. 47*, 939–947.

BI801118F